Description of even-even triaxial nuclei within the Coherent State and the Triaxial Rotation Vibration Models

U. Meyer[a], A.A. Raduta[a,b] and Amand Faessler[a]

[a)] *Institut für Theoretische Physik der Universität Tübingen, Auf der Morgenstelle 14, D-72076 Tübingen, Germany*

[b)] *Institute of Physics and Nuclear Engineering, Bucharest, POBox MG6, Romania*

(February 9, 2008)

Abstract

The coherent state model (CSM) and the triaxial rotation-vibration model (TRVM) are alternatively used to describe the ground, γ and β bands of ^{228}Th. CSM is also applied to the nuclei ^{126}Xe and ^{130}Ba, which were recently considered in TRVM. The two models are compared with respect to both their underlying assumptions and to their predicted results for energy levels and E2 branching ratios. Both models describe energies and quadrupole transitions of ^{228}Th equally well and in good agreement with experiment, if the 0_3^+ level at 1120 keV is interpreted as the head of the β band. The other two 0^+ levels at 832 and 939 keV are most likely not of a pure quadrupole vibration nature as has been already pointed out in the literature.

PACS number(s): 21.60.Ev, 23.20-g, 23.20.Js, 27.60.+j

I. INTRODUCTION

The quadrupole degrees of freedom have been intensively used by phenomenological models to interpret the data for energies and electromagnetic transitions of collective states. In the pioneering model of Bohr and Mottelson [1] (**L**iquid **D**rop **M**odel=LDM) some collective properties are treated in terms of quadrupole shape coordinates describing small oscillations of the nuclear surface around a spherical equilibrium shape.

The harmonic motion of the liquid drop and the restriction to a spherical shape for the ground state are severe limitations of this approach. The first improvement of the LDM was obtained in the rotation-vibration model (RVM) [2–5] in which the deviation of the shape coordinates from their static values is considered and by this an axially symmetric deformed shape is described. Anharmonicities were introduced by Greiner and Gneuss [6]. In this way many collective features for the complex spectra could be explained consistently.

In order to explain quantitatively the excitation energies and transition probabilities, the interacting boson approximation (IBA) exploits underlying group symmetries [7,8]. In IBA most of the nuclei have been ordered in three categories characterised by the dynamical symmetries of the model Hamiltonian. The symmetries correspond to the groups O(6), SU(5) and SU(3) and the specific features are γ-instability, γ-stability and the quasi degeneracy of states with equal angular momentum belonging to γ and β bands, respectively.

The coherent state model (CSM), developed in the beginning of the eighties, treats an effective Hamiltonian in a restricted model space generated by projecting out the angular momentum from three orthogonal and deformed states [9–18]. These are chosen as the lowest elementary boson excitations of an axially symmetric coherent state. The axially deformed picture is very convenient since it allows to define the K quantum number.

Recently, there appeared several data about triaxial deformed nuclei which were interpreted in the IBA by using its O(6) limit [19]. This was a real challenge for the RVM authors who extended the model to triaxial equilibrium shapes (**T**riaxial **R**otation-**V**ibration **M**odel=TRVM) [20]. The TRVM was applied to the nuclei ^{126}Xe and ^{130}Ba and the results obtained were in equally good

agreement with available data [19,21,22] as in IBA [20] .

A short while ago, new data for ^{228}Th were detected [23]. According to these data, ^{228}Th behaves as a nucleus without axial symmetry. Since the first successful applications of CSM referred to the Pt region [9], which corresponds to the O(6) symmetry in the IBA interpretation, it is expected that triaxial nuclei like ^{126}Xe, ^{130}Ba and ^{228}Th can be realistically described by CSM. We furthermore apply the TRVM for the new data of ^{228}Th.

We are not only interested in the predictions of the two models but we would also like to point out resemblances and differences of their theoretical ingredients. Therefore we discuss in Section 4, after a brief description of the two approaches in Sections 2 and 3, a possible relation between the two models. We present our numerical results in Section 5. Section 6 contains the final conclusions.

II. THE TRIAXIAL ROTATION VIBRATION MODEL

The RVM was extended recently [20] to triaxial nuclei (TRVM). Here we briefly present the results.

The TRVM describes small oscillations of a quadrupole deformed nuclear surface

$$R(\theta,\phi) = R_0(1 + \sum_{\mu} \alpha_{2\mu} Y^*_{2\mu}(\theta,\phi)), \tag{2.1}$$

around an ellipsoidal shape without axial symmetry. The classical Hamiltonian governing the motion of the quadrupole shape coordinates $\alpha_{2\mu}$ is given by:

$$H = \frac{1}{2} B \sum_{\mu} \dot{\alpha}^*_{2\mu} \dot{\alpha}_{2\mu} + V(\alpha_{2\mu}) \ . \tag{2.2}$$

In the intrinsic reference frame the five degrees of freedom are a_0, a_2 and Ω, where Ω denotes the Euler angles fixing the position of the intrinsic frame with respect to the laboratory frame. The a_k (k=0,2) are obtained from the coordinates α_{2k} through the rotation $\hat{R}(\Omega)$:

$$a_k = \hat{R}(\Omega) \alpha_{2k} \hat{R}(\Omega)^\dagger \quad , \quad k = 0, 2 \ . \tag{2.3}$$

In the Bohr-Mottelson parametrization, the new coordinates a_k are expressed in terms of β and γ deformations by:

$$a_0(t) = \beta\cos(\gamma),$$
$$a_2(t) = \frac{1}{\sqrt{2}}\beta\sin(\gamma). \tag{2.4}$$

The stationary points of the trajectory defined by ($a_0(t)$, $a_2(t)$, $\Omega(t)$) are identical with stationary points of the equipotential energy surface. Assuming (β_0, a_2) to be a minimum of this surface , one may deduct from the surface variables a_0 and a_2 their static parts and consider resulting deviations as new dynamical variables:

$$a_0(t) = \beta_0 + a_0'(t), \tag{2.5}$$
$$a_2(t) = a_2 + a_2'(t). \tag{2.6}$$

The new dynamical coordinates are supposed to be small comparing them to the static deformations. In this case we may expand the model Hamiltonian up the second order in a_0'/β_0 and a_2'/a_2.

After quantization, the Hamiltonian splits up into several terms which can be written as:

$$H \equiv T + V = T_{rot} + T_{vib} + T_{rotvib} + V_{\beta_0 a_2}(a_0', a_2'), \tag{2.7}$$

where the following notations have been used:

$$\begin{aligned} T_{rot} &= \frac{\hat{\mathbf{I}}^2 - \hat{I}_3^2}{2I_0} + \frac{\hat{I}_3^2}{16Ba_2^2}, \quad T_{vib} = -\frac{\hbar^2}{2B}\left(\frac{\partial^2}{\partial a_0'^2} + \frac{1}{2}\frac{\partial^2}{\partial a_2'^2}\right), \\ T_{rotvib} &= \frac{\hat{\mathbf{I}}^2 - \hat{I}_3^{\,2}}{2I_0} f_0(\beta_0, a_2, a_0', a_2') + \frac{\hat{I}_+^2 + \hat{I}_-^2}{2I_0} f_1(\beta_0, a_2, a_0', a_2') \\ &\quad + \frac{\hat{I}_3^2}{16Ba_2^2} f_2(a_2, a_2') + 2\epsilon\frac{a_0'}{\beta_0}, \\ V(a_0', a_2') &= \frac{1}{2}C_0 a_0'^2 + C_2 a_2'^2. \end{aligned} \tag{2.8}$$

The final expressions for the coefficients f_0, f_1, and f_2, obtained by the above mentioned expansion, are :

$$\begin{aligned} f_0 &= -2\frac{a_0'}{\beta_0} + 3\frac{a_0'^2}{\beta_0^2} + \frac{2}{\beta_0^2}(a_2^2 + 2a_2a_2' + a_2'^2), \\ f_1 &= \frac{1}{3}\sqrt{6}\frac{1}{\beta_0}(a_2 + a_2') - \sqrt{6}\frac{1}{\beta_0^2}a_0'(a_2 + a_2'), \\ f_2 &= -2\frac{a_2'}{a_2} + 3\frac{a_2'^2}{a_2^2}. \end{aligned} \tag{2.9}$$

The moment of inertia (I_0) is equal to $I_0 = 3B\beta_0^2$ and its inverse is denoted by $\epsilon = 1/I_0$.

The eigenstates of the unperturbed Hamiltonian

$$H_0 = T_{rot} + T_{vib} + V, \tag{2.10}$$

are taken as diagonalization basis for the coupling Hamiltonian. A basis state $|IK, n_2 n_0\rangle$ is labelled by the total angular momentum (I), its projection on the intrinsic z-axis (K) and by the number of phonons for the β (n_0) and γ (n_2) vibrations. For K=0, the angular momentum I takes only even values, whereas for K=2,4,6,... all values $I > K$ are allowed. The basis is restricted to quantum numbers $K \leq 6$ and $n_2 + n_0 \leq 2$.

The TRVM has four parameters. These are the vibration energies $E_\beta (= \hbar\sqrt{\frac{C_0}{B}})$ and $E_\gamma (= \hbar\sqrt{\frac{C_2}{B}})$, the inverse moment of inertia ϵ and the ratio a_2/β_0 of the static deformations. To these four parameters, we add the Lipas's parameter α_L [24], which corrects the incomplete description of the variation of the moment of inertia due to the restriction of the diagonalization space. The Lipas's parameter relates the excitation energies E_0, obtained by diagonalizing the model Hamiltonian, with the energies E which are to be compared with the data:

$$E = E_0/(1 + \alpha_L E_0). \tag{2.11}$$

The Lipas's parameter influences only the energies, but not the wavefunctions.

The transition probabilities can be readily obtained once we have determined the initial and final states as well as the transition operator. In Ref. [20] a compact expression for the transition operator $m(E2, \mu)$, was obtained. This is given by:

$$\begin{aligned} m(E2,\mu) = \frac{3Z}{4\pi} R_0^2 \Bigg[& \mathcal{D}^2_{\mu 0} \left(\beta_0 \left(1 + \frac{2}{7} \left(\frac{5}{\pi} \right)^{\frac{1}{2}} \beta_0 \right) \right) + \mathcal{D}^2_{\mu 0} a'_0 \left(1 + \frac{4}{7} \left(\frac{5}{\pi} \right)^{\frac{1}{2}} \beta_0 \right) + \\ & \mathcal{D}^2_{\mu 0} \frac{2}{7} \left(\frac{5}{\pi} \right)^{\frac{1}{2}} ({a'_0}^2 - 2(a_2 + a'_2)^2) + \\ & (\mathcal{D}^2_{\mu 2} + \mathcal{D}^2_{\mu -2}) \left(\left(1 - \frac{4}{7} \left(\frac{5}{\pi} \right)^{\frac{1}{2}} \beta_0 \right) (a_2 + a'_2) - \frac{4}{7} \left(\frac{5}{\pi} \right)^{\frac{1}{2}} a'_0 (a_2 + a'_2) \right) \Bigg] \end{aligned} \tag{2.12}$$

We use standard notations for the nucleus charge (Ze), nuclear radius (R_0) and Wigner's functions ($\mathcal{D}^2_{MK}$). The transition operator depends on both the static and the dynamical deformations. It

contains not only terms which are linear in a'_0 and a'_2 but also quadratic and constant terms. While the latter terms are caused by the deformation effects due to the transformations (2.5) and (2.6), the former terms reflect an anharmonic structure for the E2 transition.

III. THE COHERENT STATE MODEL

The coherent state model (CSM) was to a great part developed, in collaboration, by one of the present authors (A.A.R.) [10], with the scope to describe the main features of the collective ground, β and γ bands.

First, one defines a restricted collective space by projecting out the components with good angular momentum from three orthogonal deformed states. One of the states, Ψ_g, is a coherent state with axial symmetry describing a deformed ground state. The remaining states, denoted by Ψ_γ and Ψ_β, are obtained by exciting Ψ_g with polynomials of second and third rank in the quadrupole bosons. These are chosen in such a way that the three deformed states are mutually orthogonal. Moreover, one requires that the orthogonality is preserved after projection was performed.

The three states depend on a real parameter (d) which simulates the nuclear quadrupole deformation. Indeed, d is proportional to the expectation value of the quadrupole moment operator corresponding to the deformed ground state. As a matter of fact due to this property the attribute 'deformed state' may be assigned to the three states before projection.

In the vibrational limit ($d \to 0$) [15,16], the states projected from Ψ_g, Ψ_γ and Ψ_β are the highest seniority states, whereas in the rotational limit ($d \geq 3$) [14] they behave similarly as the liquid drop wavefunctions for the ground state, γ and β bands, respectively. The intermediate situations where K is not a good quantum number are reached by a smooth variation of the deformation parameter d. In this way one achieves a one to one correspondence between vibrational and rotational states which agrees with the semi-empirical rule of Sheline and Sakai [25,26].

In the restricted quadrupole boson space spanned by the projected states one determines an effective Hamiltonian which ideally should be diagonal in the model basis states. The simplest solution is a sixth order boson Hamiltonian which has vanishing off diagonal matrix elements for

the β band states:

$$H = A_1 \left(22\hat{N} + 5\Omega^\dagger_{\beta'}\Omega_{\beta'} \right) + A_2 \hat{I}^2 + A_3 \Omega^\dagger_\beta \Omega_\beta. \tag{3.1}$$

Here $\hat{N}$ and $\hat{I}^2$ denote the quadrupole boson number and total angular momentum squared operators, respectively. The other notations are:

$$\Omega^\dagger_{\beta'} = \left[b^\dagger_2 \times b^\dagger_2 \right]^0 - \frac{d^2}{\sqrt{5}}, \tag{3.2}$$

$$\Omega^\dagger_\beta = \left[b^\dagger_2 \times b^\dagger_2 \times b^\dagger_2 \right]^0 + \frac{3d}{\sqrt{14}} \left[b^\dagger_2 \times b^\dagger_2 \right]^0 - \frac{d^3}{\sqrt{70}}, \tag{3.3}$$

where $b^\dagger_{2\mu}$ ($-2 \leq \mu \leq 2$) are the components of the quadrupole boson operator. Consequently, the energies of the β and γ band states of odd angular momentum are given as expectation values on the corresponding projected states. The energies of ground state and gamma band states with even angular momenta are obtained by diagonalizing a 2×2 matrix. We would like to emphasize that the off-diagonal matrix elements vanish in the extreme regimes.

The reduced E2 transition probabilities are described by the anharmonic operator:

$$Q_{2\mu} = q_1 \left(b^\dagger_{2\mu} + (-1)^\mu b_{2-\mu} \right) + q_2 \left(\left[b^\dagger_2 b^\dagger_2 \right]^2_\mu + \left[b_2 b_2 \right]^2_\mu \right). \tag{3.4}$$

Rotational and vibrational limits for energies and B(E2) values have been studied analytically in Refs. [14–16]

Numerical calculations showed that the CSM describe equally well nuclei of different symmetries like O(6) (^{190,192,194}Pt), SU(3) (^{232}Th, ^{238}U) and SU(5) (^{150}Sm, ^{152}Gd). In some cases, for example for ^{156}Dy, the β band has a complex structure which can be described after adding two more terms to the CSM-Hamiltonian:

$$H' = A_4 \left(\Omega^\dagger_\beta \Omega_{\beta'} + h.c. \right) + A_5 \Omega^{\dagger\,2}_{\beta'} \Omega^2_{\beta'}. \tag{3.5}$$

which do not alter the decoupling property of the β band. The CSM was extended by including the coupling of quadrupole collective motion to the individual [11–13] as well as to the octupole degrees of freedom [14,17,18]. CSM differs from the IBA formalism in several essential features. Indeed, the model Hamiltonian is a boson number non-conserving Hamiltonian. The CSM states

are projected from an infinite series of bosons and therefore dynamical effects for any nuclear deformation and angular momentum can be accounted for. In particular, due to the coherent property of the deformed ground state, the CSM works very well for high spin states. We would like to note that the collective motion within CSM is determined by both high anharmonicities involved in the model Hamiltonian and the complex structure of the model space. The CSM is compared with the TRVM in the next Section.

IV. COMPARISON BETWEEN CSM AND TRVM

Since the deformed ground state is a vacuum state for the shifted quadrupole boson operator

$$(b_{20} - d)\Psi_g = 0, \tag{4.1}$$

and moreover the transformation e^T with $T = d\left(b^\dagger_{20} - b_{20}\right)$ produces such a shift

$$e^T b e^{-T} = b - d \ , \ \ e^T b^\dagger e^{-T} = b^\dagger - d, \tag{4.2}$$

one expects that the transformed Hamiltonian $e^T H e^{-T}$ is a deformed operator which may describe the motion around an axially deformed shape.

The classical motion of an axially non-symmetric shape can be studied by the associated classical energy function:

$$\mathcal{H} = \langle\Psi|\hat{H}|\Psi\rangle, \tag{4.3}$$

where

$$|\Psi\rangle = exp(z_0 b^\dagger_{20} + z_2 b^\dagger_{22} + z_{-2} b^\dagger_{2-2} - z^\star_0 b_{20} - z^\star_2 b_{22} - z^\star_{-2} b_{2-2})|0\rangle, \tag{4.4}$$

and $\hat{H}$ is given by (3.1). The vacuum state for the quadrupole bosons is denoted by $|0\rangle$. The coefficients $z_0, z_2, z_{-2}, z^\star_0, z^\star_2, z^\star_{-2}$ are complex functions of time and define the classical phase space coordinates. By direct calculation one finds:

$$\mathcal{H} = 2\left(11A_1 + 3A_2\right)\left(z_0 z^\star_0 + z_2 z^\star_2 + z_{-2} z^\star_{-2}\right) +$$

$$A_1\left(z_0^2+2z_2z_{-2}-d^2\right)\left(z_0^{\star\,2}+2z_2^\star z_{-2}^\star-d^2\right)+$$
$$\frac{A_3}{70}\left[2\left(6z_0z_2z_{-2}-z_0^3\right)+3d\left(z_0^2+2z_2z_{-2}\right)-d^3\right]$$
$$\left[2\left(6z_0^\star z_2^\star z_{-2}^\star-z_0^{\star\,3}\right)+3d\left(z_0^{\star\,2}+2z_2^\star z_{-2}^\star\right)-d^3\right]. \tag{4.5}$$

The motion of the phase space coordinates is governed by the equations provided by the variational principle[1]

$$\delta\int\langle\Psi|(H-i\frac{\partial}{\partial t}|\Psi\rangle dt'=0. \tag{4.6}$$

The results are:

$$\{z_k,\mathcal{H}\}=\dot{z}_k\ ,\ \{z_k^\star,\mathcal{H}\}=\dot{z}_k^\star\ ,\ \{z_k,z_{k'}^\star\}=-i\delta_{kk'}, \tag{4.7}$$

where the Poisson bracket is defined with respect to the canonically conjugate variables $(\sqrt{2}Re(z_k),\sqrt{2}Im(z_k))$.

Stationary points of this motion are also stationary points for the surface of constant energy:

$$\mathcal{H}(z_0,z_0^\star,z_2,z_2^\star,z_{-2},z_{-2}^\star)=E \tag{4.8}$$

Suppose now that this surface exhibits a minimum point $(z_0,z_2)=(u_0,u_2)$ with u_0 and u_2 being real numbers. The existence of such a minimum is proved in Ref. [27]. Since we want to mention here some classical features which do not depend on whether this minimum is axially symmetric or not we consider the simplifying case u_2=0. Expanding $\mathcal{H}$ around the minimum point and keeping only the quadratic terms in the deviations $z_k',z_k^{\star\,\prime}$, one obtains:

$$\mathcal{H}=\mathcal{H}_0+\mathcal{H}_\beta+\mathcal{H}_\gamma. \tag{4.9}$$

where $\mathcal{H}_0$ is a constant term (not depending on coordinates) and

$$\mathcal{H}_\beta=B_1z_0'z_0^{\star\,\prime}+B_2\left(z_0'^{\,2},+(z_0^{\star\,\prime})^2\right)\ , \tag{4.10}$$
$$\mathcal{H}_\gamma=G_1\left(z_2'z_2^{\star\,\prime}+z_{-2}'z_{-2}^{\star\,\prime}\right)+G_2\left(z_2'z_{-2}'+z_2^{\star\,\prime}z_{-2}^{\star\,\prime}\right), \tag{4.11}$$

[1]We use the units $\hbar$=c=1

The coefficients B_1, B_2, G_1 and G_2 are explicitly given in Appendix A. Note that at the level of quadratic approximation there is no $\beta - \gamma$ coupling term.

The classical motion can be quantized as follows. One defines first a new set of coordinates and momenta:

$$Q_2 = \frac{1}{\sqrt{2}}(z_2^\star + z_{-2}), Q_{-2} = \tfrac{1}{\sqrt{2}}(z_{-2}^\star + z_2), Q_0 = \frac{1}{\sqrt{2}}(z_0^\star + z_0), \tag{4.12}$$

$$P_2 = \frac{i}{\sqrt{2}}(z_{-2}^\star + z_2), P_{-2} = \tfrac{i}{\sqrt{2}}(z_2^\star + z_{-2}), P_0 = -i\frac{\partial}{\partial Q_0}. \tag{4.13}$$

The Poisson brackets of these coordinates can be easily calculated and the result reflects their canonically conjugate character:

$$\{Q_k, P_{k'}\} = \delta_{kk'} \ , \ \ k = 0, \pm 2 \ . \tag{4.14}$$

For small deviations from the minimum point, it is useful to introduce the parametrization:

$$Q_{\pm 2} = \frac{\gamma}{\sqrt{2}}\, e^{\pm 2i\phi} \equiv \frac{q_{\pm 2}}{\sqrt{2}} \tag{4.15}$$

Let us consider as coordinate operators the Q_k as defined above, but denoted hereafter by $\hat{Q}_k$, and the corresponding momenta defined by:

$$\hat{P}_{\pm 2} = -\frac{i}{\sqrt{2}}\frac{\partial}{\partial q_{\pm 2}} \ , \ \ \hat{P}_0 = -i\frac{\partial}{\partial Q_0} \tag{4.16}$$

Indeed, one can easily check that

$$\left[\hat{Q}_{\pm 2}, \hat{P}_{\pm 2}\right] = 1 \tag{4.17}$$

The transformation $(Q_{\pm 2}, P_{\pm 2}) \rightarrow (\hat{Q}_{\pm 2}, \hat{P}_{\pm 2})$ is usually called canonical quantization. Quantized Hamiltonians are obtained by writing $\mathcal{H}_\beta$ and $\mathcal{H}_\gamma$ in terms of $(Q_{\pm 2}, P_{\pm 2})$ and then making the above mentioned replacements. The latter transformation is made after putting the mixed Q and P terms in a symmetrized form. The final results are:

$$\hat{H}_\gamma = -\frac{1}{2}(G_1 - G_2)(\frac{\partial^2}{\partial\gamma^2} + \frac{1}{\gamma}\frac{\partial}{\partial\gamma} + \frac{1}{4\gamma^2}\frac{\partial^2}{\partial\phi^2}) + \frac{G_1 + G_2}{2}\gamma^2 \tag{4.18}$$

$$\hat{H}_\beta = -\frac{1}{2}\,(B_1 - 2B_2)\,\frac{\partial^2}{\partial Q_0^2} + \frac{1}{2}(B_1 + 2B_2)Q_0^2 \tag{4.19}$$

The spectra which are obtained with the above two operators, H_β and H_γ, are:

$$E_N^{(\gamma)} = \omega_\gamma(N+1) \ , \ \ N = 2n + \frac{1}{2}|K| \ , \ \ n = 0,1,2,\ldots \ \ |K| = 0,2,4,\ldots \tag{4.20}$$

$$E_n^{(\beta)} = \omega_\beta\left(n + \frac{1}{2}\right) \ , \ \ n = 0,1,2,\ldots \tag{4.21}$$

where

$$\omega_\gamma = \left(G_1^2 - G_2^2\right)^{1/2} \ , \ \omega_\beta = \left(B_1^2 - 4B_2^2\right)^{1/2} \tag{4.22}$$

Inspecting the expressions from Appendix A, one sees that G_1 and B_1 are mainly given by the $\hat{N}$ term of the model Hamiltonian. Indeed, the coefficient A_2 accompanying $\hat{I}^2$ is usually small. Therefore, the γ and β harmonic frequencies are decreased by anharmonicities.

Although we discuss the simplest case, the γ degree of freedom could not be decoupled entirely from the rotational coordinate ϕ. This seems to be a general feature for the liquid drop model.

The Hamiltonian $\hat{H}_\beta + \hat{H}_\gamma$ is similar to the part $T_{vib} + T_{rotvib} + V$ of the TRVM except for the coupling terms. Indeed, here only one coupling term is reproduced. The reason is that by restricting the coherent state to the $b_{20}^\dagger, b_{22}^\dagger, b_{2-2}^\dagger$ bosons, the motion of two Euler angles is not taken into account. If we considered the coherent states of five variables as the variational state, the TRVM Hamiltonian would have been entirely obtained, as the harmonic limit, by the procedure described above.

The fact that the classical picture leads to the interpretation of the generating deformed states given below is remarkable. Under circumstances of small deviations from the equilibrium shape the one beta and one gamma phonon states can be written in the form of Ψ_β and Ψ_γ, respectively [27]. Thus, one may assert that by means of projection technique the CSM builds up rotational bands on the top of three deformed states which represent the ground, beta and gamma one phonon states, respectively. The CSM uses a highly anharmonic Hamiltonian and the projected states are superpositions of all K quantum numbers. This results in generating some important effects for high spin states. By contradistinction, TRVM uses a harmonic vibrational Hamiltonian and a diagonalization basis subject to the restriction $K \leq 6$. On the other hand, one can easily describe multi-phonon states as well as $K \neq 0, 2$ rotational bands in the TRVM. To adapt the CSM to higher excited bands would require a great amount of additional effort.

V. NUMERICAL RESULTS

The CSM and TRVM have been applied to three triaxial nuclei: ^{126}Xe, ^{130}Ba and ^{228}Th. Although the TRVM has been already considered for the first two nuclei, for the sake of a complete comparison between the two models we also invoke these results in the present paper.

The parameters obtained through a fitting procedure have been collected in Table 1. The TRVM fixes its parameters so that a best overall fit for the experimental excitation energies is obtained. The CSM fitting procedure is as follows. For a given d, A_1 and A_2 are determined so that the excitation energies for 2_g^+ and 2_γ^+ are equal to the corresponding experimental data. The parameter A_3 is used to fit the excitation energy for 0_β^+. Finally, one keeps that value of d which assures an overall best fit for the excitation energies in the three bands. The CSM uses a transition operator which depends on two parameters, q_0 and q_2. Since one deals with branching ratios, only one is needed. Therefore we give here the ratio $\frac{q_2}{q_0}$. The branching ratios depend also on the deformation parameter d, which was already determined from energy analyses.

Note that for ^{126}Xe and ^{130}Ba, the best fit is obtained, within TRVM, if one assumes that the 0_2^+ band is a $K^\pi = 0^+$ gamma band . Another feature revealed by the TRVM parameters consists of that, except for ^{130}Ba, where E_β and E_γ are nearly degenerate, the beta band is higher in energy than gamma band, which reflects a gamma unstable picture or, in other words saying, an $O(6)$ symmetry. The property mentioned above for the excepting case recommends ^{130}Ba as a representative of $SU(3)$. As seen from the row corresponding to the parameter d, ^{126}Xe and ^{130}Ba are weakly deformed nuclei while ^{228}Th is a well deformed nucleus. The static values of the γ deformation, extracted from the a_2/β_0 values given in the Table 1, are about 25^0 for ^{126}Xe and ^{130}Ba and 13^0 for ^{228}Th.

Although CSM uses a b_{20}^+-coherent state for the unprojected ground state, the I-projected states are superpositions of the functions $\mathcal{D}_{MK}^{I\star}$ with the expansion coefficients $A_{\alpha IK}(\beta\gamma)$ depending on the β and γ deformations. Integrating over β, the square of these coefficients, a probability distribution for the gamma variable is obtained. Such investigations can also be performed in connection with the projected states associated to beta and gamma bands. Since the details of

this analysis can be found in Ref. [28], we only enumerate the main results. The 0_g^+ state behaves as a gamma unstable wavefunction while the ground band states of high spin, like 10_g^+, has a gamma probability with a maximum at 45^0. The γ band state 2_γ^+ describes a triaxial nucleus ($\gamma = 30^0$) while increasing the spin the probability distribution in the variable γ goes gradually to the situation when it has two equal maxima at 0^0 and 60^0. In conclusion, the γ asymmetric features are in CSM accounted for due to the mixture of ground and gamma projected states as well as due to the specific anharmonic structure of the model Hamiltonian.

It is instructive to compare the experimental results for the sum of energies for the first two states of angular momentum two and the energy of the first 3^+ state. The differences are about 2, 47 and 95 keV for ^{228}Th, ^{126}Xe and ^{130}Ba , respectively. These figures suggest that ^{228}Th could be described as an asymmetric rotator [29] and therefore a decoupling regime for the β band is expected. The deviation from the rotor picture for ^{126}Xe and ^{130}Ba reflects an additional interaction between the states of ground and gamma bands.

Predicted and experimental energies of ground and gamma bands are plotted in Figures 1-3. Since only few data are available for the beta band, we summarise the results in Table 2. As seen from Table 2, within the CSM the energy spacings in the beta band are too large and this happens due to the magnitude of the A_2 coefficient. In this case the inclusion of one additional term from H' (3.5) is necessary. Indeed considering only the A_4 term and fixing its strength as to fit the energy of the 4^+ state the final results for the other states in the beta band are close to those given by the TRVM. In Ref. [23], three $K^\pi = 0^+$ bands at 832, 939 and 1120 keV have been identified. In both models, TRVM and CSM, the available data for transition probabilities could be fairly well described when the 0_3^+ band is interpreted as the beta band. This is consistent with some earlier investigations [30] pointing to the fact that the two lower bands, with $K^\pi = 0^+$, are mainly two octupole phonon and two quasiparticle states. Indeed, taking into account that the first 3^- state lies at 396 keV, the state 0_1^+ has an excitation energy close to that characterising the two octupole phonon state.

It is worth noting that by an language abuse the bands considered here are called K^π bands. Indeed, in both models, K is not a good quantum number, the eigenstates being superpositions

of several K-components. However in this superposition one K prevails and furthermore this K is taken as a band label.

An interesting feature, related to the gamma band, concerns the staggering of the $(I^+, (I+1)^+)$ states with $I \geq 3$ in ^{126}Xe and ^{130}Ba. This appears in the low part of the spectrum and more pronounced in ^{130}Ba. In CSM the staggering is a reminiscence of the vibrational limit (see Fig.3 of Ref. [10]) where the staggered states are degenerate. Beyond a critical value of d, the staggering $(3^+, 4^+), (5^+, 6^+), (7^+, 8^+)$,.., etc. which characterises the near vibrational states, changes to $(2^+, 3^+), (4^+, 5^+), (6^+, 7^+)$,..., etc. which is specific for the rotational limit. In TRVM the staggering is caused by the rotation vibration coupling terms. The spacings of the lowest two doublets are larger than those shown by experiment, in both models. We could decrease these spacings, in CSM, choosing a smaller deformation parameter d with the price of perturbing some branching ratios. However the agreement with experiment is better in the high spin region while for TRVM the discrepancies increase with angular momentum.

Within TRVM and CSM, the branching ratios characterising the decay of states belonging to the aside bands β and γ are described by means of the transition operators (2.11) and (3.4) respectively, with the parameters determined from energy analyses. In the case of CSM, there is a parameter more, $\frac{q_2}{q_0}$, which is fixed so that the experimental data for the branching ratio $(2^+_\gamma \to 0^+_g)/(2^+_\gamma \to 2^+_g)$ is reproduced.

Note that the CSM does not include the anharmonic term $[b^\dagger b]^2_\mu$ in the expression of the transition operator. The reason is that this term gives vanishing contribution to transitions between beta and ground bands. Also the transitions characterising the gamma band are affected only by a negligible amount. The results of our calculations and experimental data are given, for comparison, in Tables 3-5. The notations we used in these Tables are the standard ones. Thus for ^{126}Xe and ^{130}Ba, I^+_1, I^+_2, with I-even, stand for states of ground and gamma bands respectively, while I^+_3 (I-even) is a state from the $K^\pi = 0^+$-gamma band in the TRVM and from beta band in the CSM. If I is odd, I^+_1 is a state from the gamma band. As we have already mentioned , ^{228}Th exhibits three excited $K^\pi = 0^+$ bands. The best agreement for branching ratios are obtained interpreting the 0^+_3 band as the beta band. This implies the following notations for ^{228}Th. The

states I_4^+ with I=even belong to the gamma band while the states of beta band are of the type I_5^+. Exception is for the state 2^+ of the gamma band which is the third state of angular momentum 2.

From tables 3-5 one may see that both models describe reasonably well the data reffering to the gamma band. The agreement quality for the two models are comparable. One should mention that within TRVM, branching ratios associated to the state 2_3^+ of ^{126}Xe and ^{130}Ba are much smaller than the corresponding data, while CSM predictions lie quite close to the experimental data. In ^{130}Ba, the normalised transitions $4_3^+ \rightarrow 2_2^+$, $4_3^+ \rightarrow 2_1^+$ predicted by TRVM exceed the experimental data by a factor of about 231 and 132 respectively while CSM results underestimate the data by a factor of 5 and 4.3, respectively. These data suggest that additional terms in the TRVM Hamiltonian are necessary in order to improve the structure of the eigenfunctions describing the above mentioned decaying states. The results obtained in both models for ^{228}Th agree quite well with each other as well as with the experimental data. Moreover, the realistic description of the data concerning the decay of the states 2_5^+ and 4_5^+ support our assignment of the beta band to the experimental 0_3^+ band.

VI. CONCLUSIONS

In the previous sections two phenomenological models, CSM and TRVM, have been successively applied to three triaxial nuclei : ^{126}Xe, ^{130}Ba and ^{228}Th. While the second model was adapted for triaxial nuclei in a previous publication, the original CSM was applied without any modification. One suggests a possible relation between the two models. Indeed, the TRVM seems to be the classical counterpart of the CSM in the harmonic limit. The proof for this relationship has the virtue of suggesting a way of supplementing the Hamiltonian characterising the TRVM with some anharmonic terms.

The two models yield similarly good results concerning the excitation energies and transition probabilities for ^{228}Th. Moreover they are at par concerning the interpretation of the 0_3^+ band as the beta band. For the remaining two nuclei the considered models are at variance with respect to the interpretation of the first excited 0^+ band. Indeed the TRVM describes the first excited

$K^\pi = 0^+$ band as a gamma band, i.e. build upon a gamma vibration state, while within the CSM this is a beta band. This difference in interpretation has an echo in the predicted branching ratio characterising the states of this band. One suggests that including anharmonicities in the TRVM Hamiltonian, the discrepancies for branching ratios might be removed.

While TRVM can be easily used for describing higher K-bands build on the top of a many phonon state, the extension of the CSM to several bands requires a good deal of additional work.

VII. APPENDIX A

Here we give the explicit expressions of the coefficients G_1, G_2, B_1, B_2 involved in the equations (4.18), (4.19) defining the γ and β vibrations.

$$
\begin{aligned}
G_1 &= 22A_1 + 6A_2, \\
G_2 &= 2A_1(u_0^2 - d^2) - \frac{3A_3}{35}(d + 2u_0)(u_0 - d)(2u_0 - du_0 - d^2), \\
B_1 &= 22A_1 + 6A_2 + 4A_1u_0^2 + \frac{18}{35}A_3u_0^2(d - u_0)^2, \\
B_2 &= A_1(u_0^2 - d^2) - \frac{3A_3}{70}(d - 2u_0)(u_0 - d)(2u_0 - du_0 - d^2).
\end{aligned} \tag{7.1}
$$

REFERENCES

[1] A. Bohr and B. Mottelson, Kgl. Danske Videnskab. Selskab Mat. Fys. **27** (1953) No16.

[2] A. Faessler, W. Greiner, Z. Phys. **168** (1962) 425.

[3] A. Faessler, W. Greiner, Z. Phys. **170** (1962) 105 and **177** (1964) 190.

[4] A. Faessler, W. Greiner, R.K. Sheline, Nucl. Phys. **70** (1965) 33.

[5] A. Faessler, W. Greiner, R.K. Sheline, Phys. Rev. **135** (1964) B591 and Nucl. Phys. **62** (1965) 241.

[6] G. Gneuss, U. Mosel and W. Greiner, Phys. Lett. **B30** (1969) 397.

[7] A. Arima and F. Iachello, Ann. Phys. **99** (1976) 253; **111** (1978) 201, **115** (1978) 325.

[8] A. Arima and F. Iachello, Phys. Rev. Lett. **40** (1978) 6, 385.

[9] A. A. Raduta, V. Ceausescu, A. Gheorghe, R. Dreizler, Phys. Lett. **99B** (1981) 444.

[10] A.A. Raduta, V. Ceausescu, A. Gheorghe, R. Dreizler, Nucl. Phys. **A381** (1982) 253.

[11] A. A. Raduta, C. Lima and Amand Faessler, Phys. Lett. **121B** (1983) 1.

[12] A. A. Raduta, C. Lima and Amand Faessler, Z. Physik **A313** (1983) 69.

[13] A. A. Raduta and S. S. Stoica, Z. Physik **A327** (1987) 275.

[14] A. A. Raduta and C. Sabac, Ann. Phys. **148** (1983) 1.

[15] A. A. Raduta, Rev. Roum. Phys. **28** (1983) 195.

[16] A. A. Raduta, C. Sabac and S. Stoica, Rev. Roum. Phys. **29** (1984) 55.

[17] A. A. Raduta, N. Lo Iudice and I. I. Ursu, Nucl. Phys. **A600** (1996) 11.

[18] A. A. Raduta, Al. H. Raduta and Amand Faessler, Phys. Rev. **C 55** (1997) 1747 .

[19] K. Kirch, G. Siems, M. Eschenauer, A. Gelberg, R. Kühn, A. Mertens, U. Neuneyer, O. Vogel, I. Wiedenhöver, P. von Brentano, T. Otsuka, Nucl. Phys. **A587** (1995) 211.

[20] U. Meyer, Amand Faessler, S.B. Khadkikar, Nucl. Phys. **A624** (1997) 391, Prog. Part. Nucl. Phys. **38** (1997) 241.

[21] G. Siems,U. Neuneyer, I. Wiedenhover,A. Albers, R. Wirowski, A. Gelberg and P. von Bretano, Phys. Lett. **B320** (1994) 1.

[22] F. Seiffert, W. Lieberz, A. Dewald, S. Freund, A. Gelberg, A. Granderath, D. Lieberz, R. Wirowski and P. von Brentano, Nucl. Phys. **A554** (1993) 287.

[23] H. Baltzer, J. de Boer, A. Gollwitzer, G. Graw, C. Günther, A.I. Levon, M. Loewe, H.J. Maier, J. Manns, U. Müller, B.D. Valnion, T. Weber, M. Würkner, Z. Phys. **A356** (1996) 13; T. Weber, J. deBoer, K. Freitag, J. Gröger, C. Günther, J. Manns, U. Müller, Z. Phys. **A358** (1997) 281; H. Baltzer (1998), private communication.

[24] P. Holmberg und P.O. Lipas, Nucl. Phys. **A117** (1968) 552.

[25] R. K. Sheline, Rev. Mod. Phys. **32** (1960) 1.

[26] M. Sakai, Nucl. Phys. **A104** (1976) 301; Nuclear Data Tables **A10** (1972) 511.

[27] A. A. Raduta and V. Baran, to be published.

[28] A. A. Raduta, Amand Faessler, Th. Koppel and C. Lima, Z. Physik **A312**(1983)233.

[29] A. S. Davydov and G. F. Filippov, Nucl Phys. **8** (1958) 237.

[30] J. Dalmasso, H. Maria and G. Ardisson, Phys. Rev. **C36** (1987) 2510.

Table Captions

Table 1. Parameters used by the TRVM (the first 5) and the CSM (the last 5) to describe the data for ^{126}Xe, ^{130}Ba and ^{228}Th. Their significance is explained in the text.

Table 2. Experimental (first column) and predicted excitation energies (in units of keV) of the 0_2^+ band given by the TRVM (second column) and the CSM (third column).

Table 3. B(E2) branching ratios for ^{126}Xe in the triaxial Rot-Vib Model (TRVM) (first column) and in the Coherent State Model (CSM) (third column) compared with experiment (second column)

Table 4. The same as in Table 3 but for ^{130}Ba.

Table 5. The same as in Table 3 but for ^{228}Th.

Figure Captions

Fig. 1. The experimental (exp.), the TRVM and CSM predicted excitation energies for ^{126}Xe are represented in units of keV for ground (**a)**) and gamma bands (**b)**).

Fig. 2. The same as in Fig. 1 but for ^{130}Ba.

Fig. 3. The same as in Fig. 1 but for ^{228}Th.

Table 1

	^{126}Xe	^{130}Ba	^{228}Th
E_β (keV)	1769	1168	1120
E_γ (keV)	1314	1179	645
ϵ (keV)	81.3	80.5	17.54
a_{20}/β_0	0.333	0.329	0.1585
α_L (keV^{-1})	10^{-4}	10^{-4}	10^{-4}
d	1.46	1.32	3.14
A_1 (keV)	14.325	15.783	17.731
A_2 (keV)	19.211	12.377	1.512
A_3 (keV)	14.411	-0.423	-7.021
q_2/q_0	-0.119	0.073	-0.071

Table 2

	^{126}Xe			^{130}Ba			^{228}Th		
	Exp.	TRVM	CSM	Exp.	TRVM	CSM	Exp.	TRVM	CSM
0^+	1314	1314	1314	1179	1179	1179	1120	1120	1120
2^+	1679	1600	1670	1557	1490	1523	1176	1173	1170
4^+	2042	2150	2254		2053	2017	1290	1292	1283
6^+		2758	3025		2644	2635		1468	1454
8^+		2917	3968		3196	3365		1690	1679
10^+		3518	5074		3947	4200		1946	1949

Table 3

$I_i \to I_f$	TRVM	exp. [22]	CSM
$2_2^+ \to 0_1^+$	8.7	1.5 ± 0.4	1.5
2_1^+	100.0	100.0	100.0
$3_1^+ \to 2_2^+$	100.0	100.0	100.0
4_1^+	24	34.0^{+10}_{-34}	13
2_1^+	4.4	$2.0^{+0.6}_{-1.7}$	1.25
$4_2^+ \to 2_2^+$	100.0	100.0	100.0
4_1^+	66	76.0 ± 22.0	76
2_1^+	1.5	0.4 ± 0.1	5.5
$0_2^+ \to 2_2^+$	100.0	100.0	100.0
2_1^+	1.1	7.7 ± 2.2	1.1
$2_3^+ \to 0_2^+$	100.0	100.0	100.0
2_2^+	0.8	$2.2 \pm 1.0^*$	3.14
4_1^+	0.04	2.0 ± 0.8	0.21
2_1^+	0.01	$0.14 \pm 0.06^*$	0.18
0_1^+	0.01	0.13 ± 0.04	0.04
3_1^+	20	$67.0 \pm 22.0^*$	20
$5_1^+ \to 6_1^+$	43	75 ± 23	25
4_2^+	83	76 ± 21	84
3_1^+	100.0	100.0	100.0
4_1^+	0.8	2.9 ± 0.8	0.15
$6_2^+ \to 6_1^+$	22	34^{+15}_{-25}	64
4_2^+	100.0	100.0	100.0
4_1^+	1.3	0.49 ± 0.15	9.99
$7_1^+ \to 6_2^+$	22	40 ± 26	31
5_1^+	100.0	100.0	100.0

Table 4

$I_i \to I_f$	TRVM	exp. [19]	CSM
$2_2^+ \to 0_1^+$	4.5	6.2 ± 0.7	6.2
2_1^+	100.0	100.0	100.0
$3_1^+ \to 2_2^+$	100.0	100.0	100.0
4_1^+	16	22.0 ± 3.0	23
2_1^+	2.6	4.5 ± 0.6	9.0
$4_2^+ \to 2_2^+$	100.0	100.0	100.0
4_1^+	57	54.0 ± 10.0	181
2_1^+	2.75	2.3 ± 0.4	0.29
$0_2^+ \to 2_2^+$	100.0	100.0	100.0
2_1^+	3.0	3.3 ± 0.2	2.2
$2_3^+ \to 0_2^+$	100.0	100.0	100.0
2_2^+	0.04	21.0 ± 4.0	20.13
4_1^+	0.11	2.7 ± 0.5	1.49
2_1^+	0.06	3.3 ± 0.6	0.005
0_1^+	0.04	0.017 ± 0.003	0.016
3_1^+	18		59
$4_3^+ \to 2_2^+$	670	2.9(5)	0.56
3_1^+	214	97(17)	17
4_2^+	100.0	100.0^*	100.0
4_1^+	7.2	$3.4(6)^*$	0.47
2_1^+	23.3	0.30(6)	0.07

Table 5

$I_i \to I_f$	TRVM	exp. [23]	CSM
$2_3^+ \to 0_1^+$	54	45(3)	45
2_1^+	100.0	100.0	100.0
4_1^+	6.1	3.1(3)	6.4
$3_1^+ \to 2_1^+$	100.0	100.0	100.0
4_1^+	62	67(6)	80
$4_4^+ \to 2_1^+$	15.1	15.0(1.2)	3.25
4_1^+	100.0	100.0	100.0
6_1^+	8.84	6.2(1.4)	1.73
$5_1^+ \to 4_1^+$	100.0	100.0	100.0
6_1^+	112	142(32)	169
$2_5^+ \to 0_1^+$	65	41(10)	59
2_1^+	100.0	100.0	100.0
4_1^+	267	420(60)	187
$4_5^+ \to 4_1^+$	100.0	100.0	100.0
6_1^+	362	470(240)	149

Figure 1a)

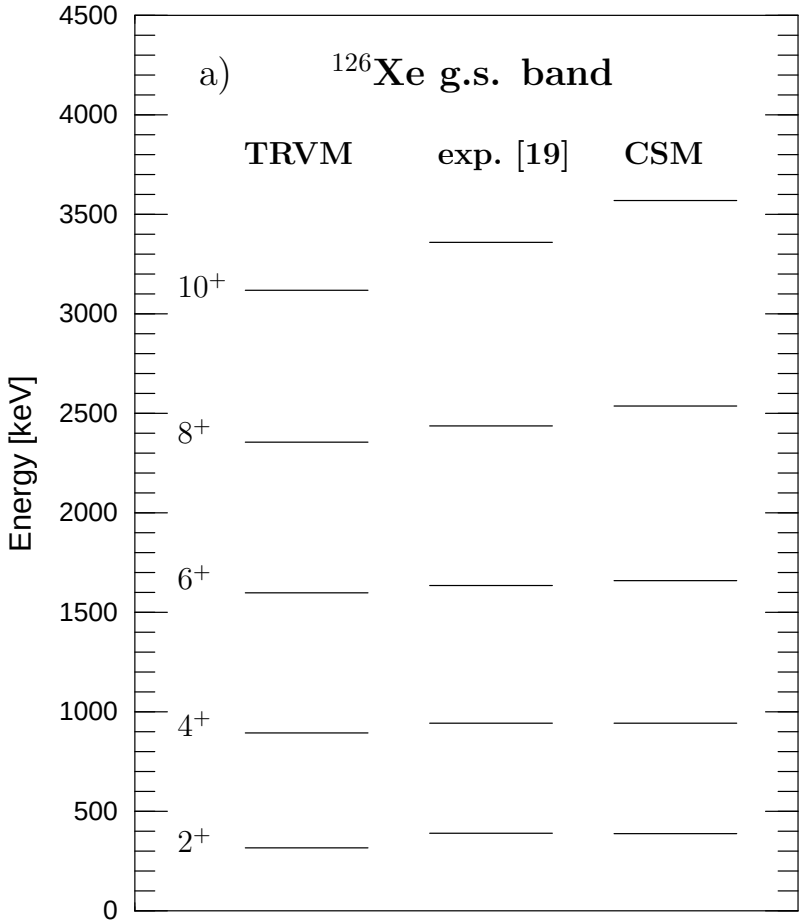
a)
^{126}Xe g.s. band
TRVM
exp. [19]
CSM
10^+
8^+
6^+
4^+
2^+
Energy [keV]
4500
4000
3500
3000
2500
2000
1500
1000
500
0

Figure 1b)

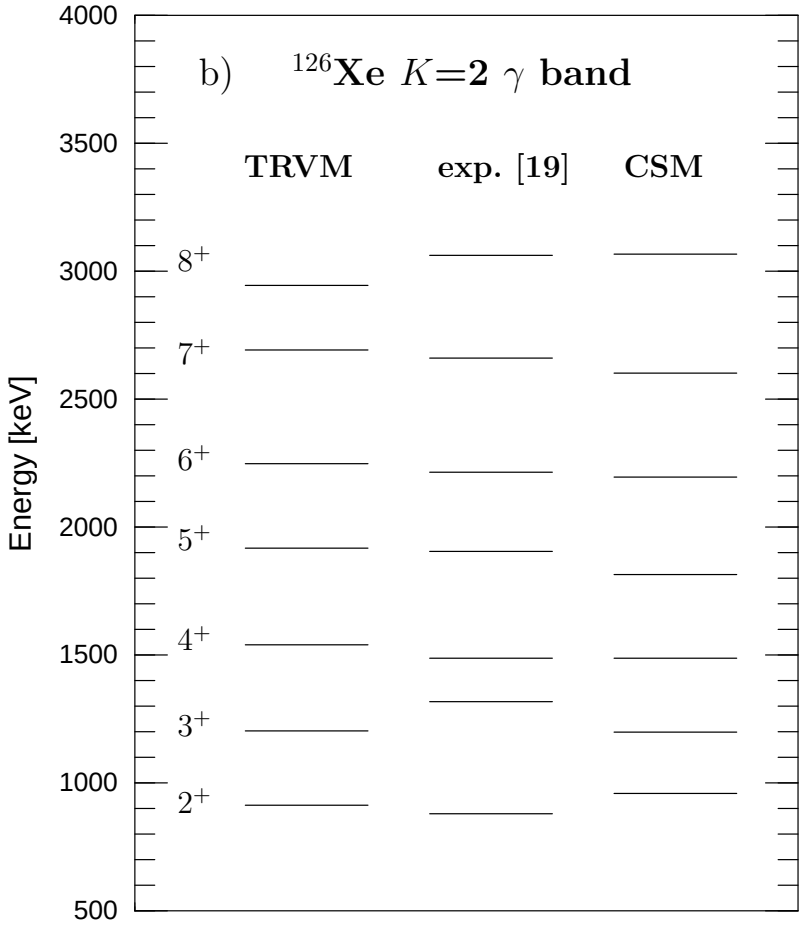
b) ^{126}Xe K=2 γ band
TRVM
exp. [19]
CSM
Energy [keV]
4000
3500
3000
2500
2000
1500
1000
500
8^+
7^+
6^+
5^+
4^+
3^+
2^+

Figure 2a)

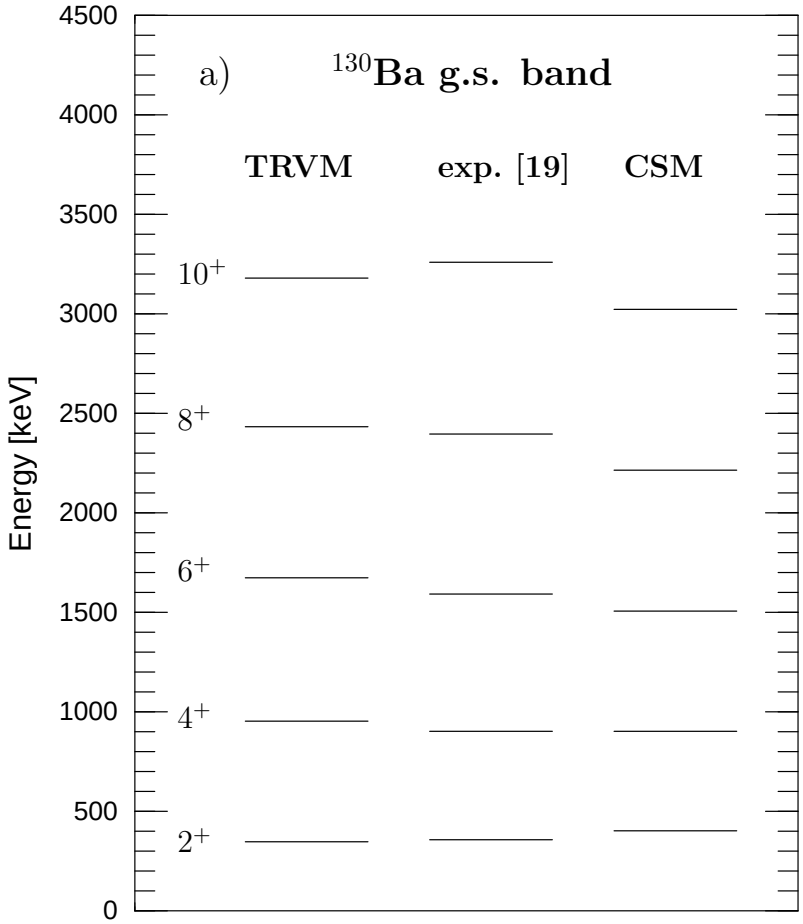
a)
^{130}Ba g.s. band
TRVM
exp. [19]
CSM
10^+
8^+
6^+
4^+
2^+
Energy [keV]
4500
4000
3500
3000
2500
2000
1500
1000
500
0

Figure 2b)

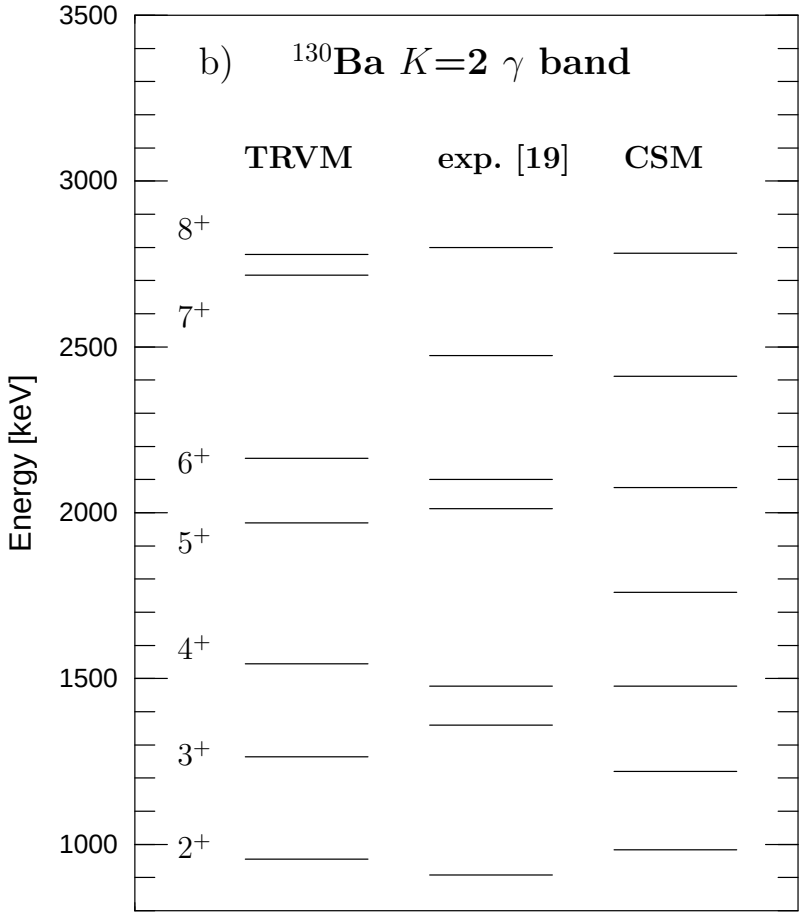
b) ^{130}Ba K=2 γ band
TRVM
exp. [19]
CSM
Energy [keV]
3500
3000
2500
2000
1500
1000
8^+
7^+
6^+
5^+
4^+
3^+
2^+

Figure 3a)

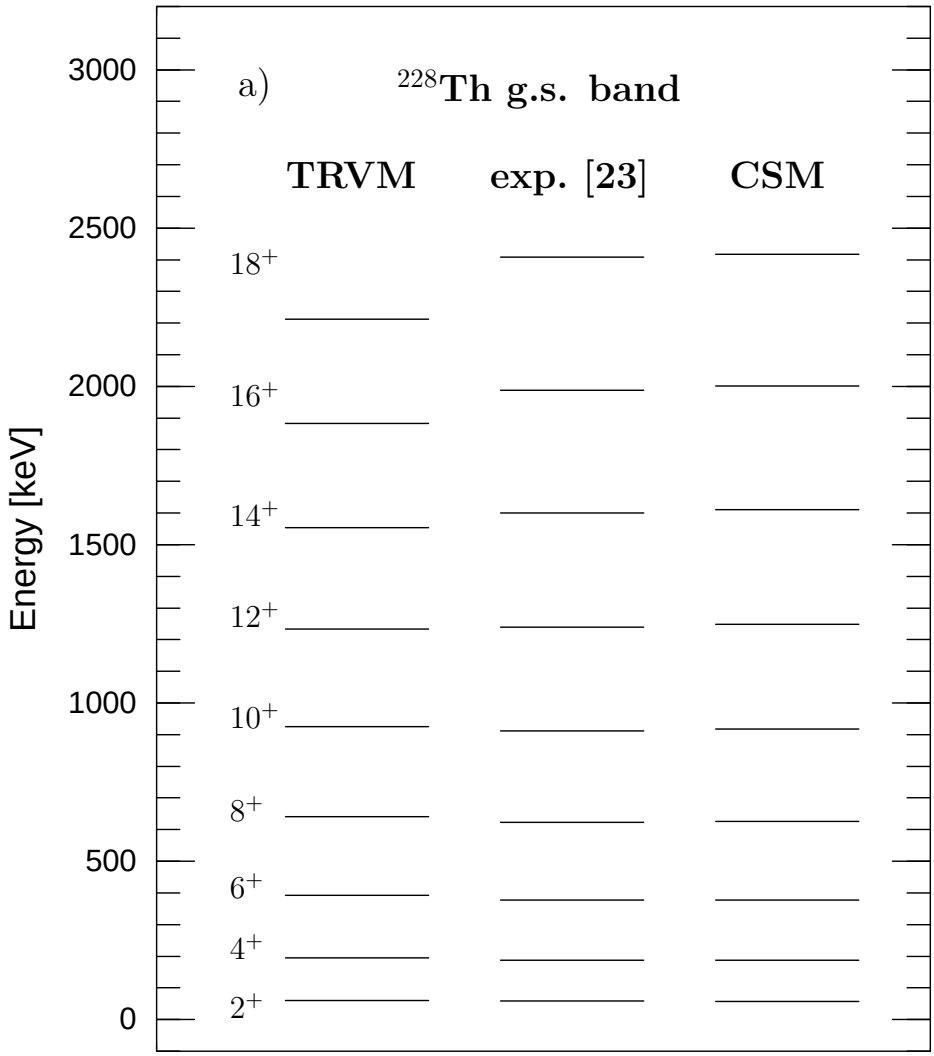
a)
^{228}Th g.s. band
TRVM
exp. [23]
CSM
Energy [keV]
3000
2500
2000
1500
1000
500
0
18^+
16^+
14^+
12^+
10^+
8^+
6^+
4^+
2^+

Figure 3b)

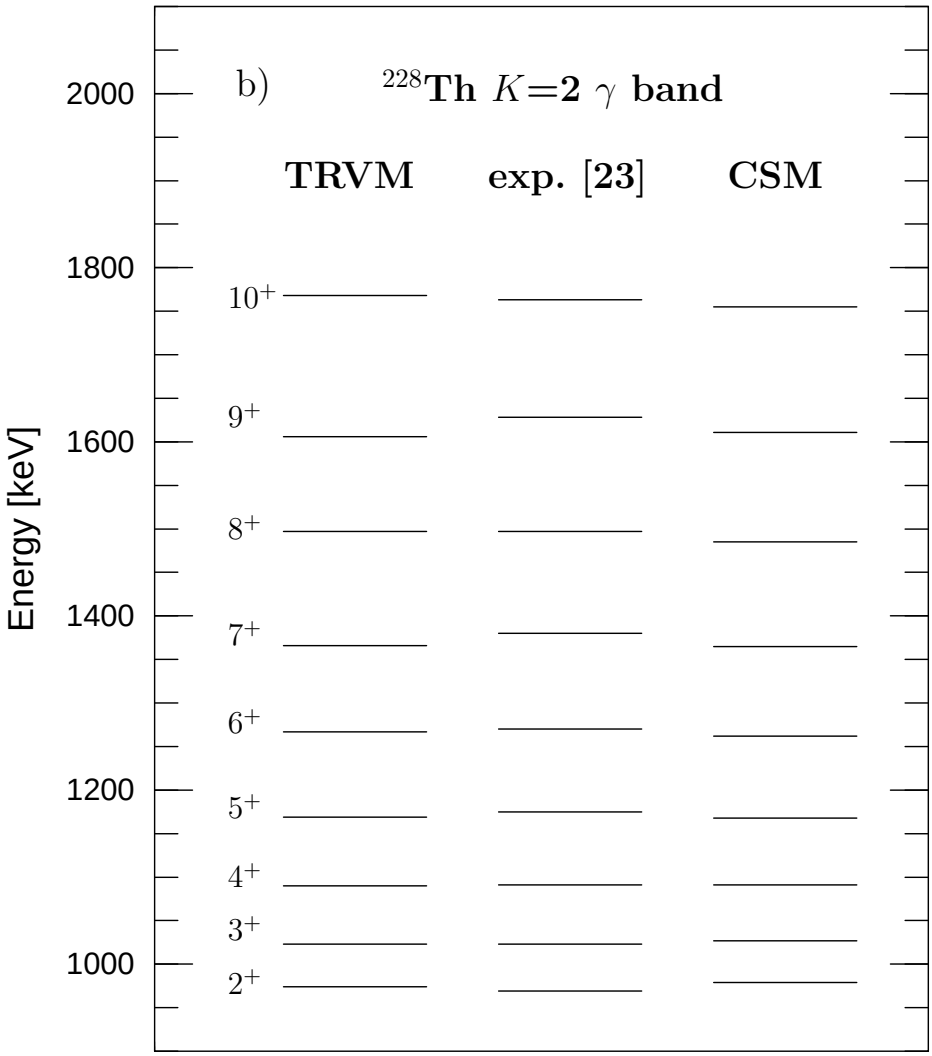
b)
^{228}Th K=2 γ band
TRVM
exp. [23]
CSM
Energy [keV]
2000
1800
1600
1400
1200
1000
10^+
9^+
8^+
7^+
6^+
5^+
4^+
3^+
2^+